
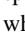

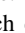


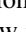
Effect of magnetic order on longitudinal Tomonaga-Luttinger liquid spin dynamics in weakly coupled spin- $\frac{1}{2}$ chains

L. Shen ,* A. Alshemi , E. Campillo , and E. Blackburn [†]

Division of Synchrotron Radiation Research, Lund University, SE-22100 Lund, Sweden

P. Steffens and M. Boehm

Institut Laue-Langevin, 71 Avenue des Martyrs, 38042 Grenoble Cedex 9, France

D. Prabhakaran and A. T. Boothroyd 

Department of Physics, University of Oxford, Clarendon Laboratory, Oxford OX1 3PU, United Kingdom



(Received 9 November 2022; revised 13 March 2023; accepted 6 April 2023; published 20 April 2023)

The quantum many-body interactions in one-dimensional spin- $\frac{1}{2}$ systems are subject to Tomonaga-Luttinger liquid (TLL) physics, which predict an array of multiparticle excitations that form continua in momentum-energy space. Here we use inelastic neutron spectroscopy to study the TLL spin dynamics in $\text{SrCo}_2\text{V}_2\text{O}_8$, a compound which contains weakly coupled spin- $\frac{1}{2}$ chains of Co atoms, at 0.05 K and in a longitudinal magnetic field up to 9.0 T. The measurements were performed above 3.9 T, where the ground-state Néel antiferromagnetic (AFM) order is completely suppressed and the multiparticle excitations are exclusively of the TLL type. In this region and below 7.0 T, the longitudinal TLL mode—psinon/antipsinon (P/AP)—is unexpectedly well described by a damped harmonic oscillator (DHO) while approaching the zone center defining the static spin-spin correlations. A non-DHO-type, continuumlike signal is seen at higher fields, but deviations from the ideal one-dimensional TLL still remain. This change in the P/AP mode coincides with the phase transition between the longitudinal spin density wave (LSDW) and transverse AFM order. Inside the LSDW state, the DHO-type P/AP spectral weight increases and the linewidth broadens as the magnetic order parameter decreases. These results reveal the impact of three-dimensional magnetic order on the TLL spin dynamics; they call for beyond-mean-field treatment for the interchain exchange interactions.

DOI: [10.1103/PhysRevB.107.134425](https://doi.org/10.1103/PhysRevB.107.134425)

I. INTRODUCTION

The Tomonaga-Luttinger liquid (TLL) theory describes interactions in one dimension (1D) [1]. From this theory, the spatial spin-spin correlation functions of an *isolated* spin- $\frac{1}{2}$ chain are expected to show power-law decays [2]. The transverse correlation function should be

$$\langle S_0^x S_r^x \rangle \approx (-1)^r r^{-\eta} \quad (1)$$

and the longitudinal correlation function should be

$$\langle S_0^z S_r^z \rangle - M_z^2 \approx \cos(2k_F r) r^{-1/\eta}, \quad (2)$$

where x and z are the directions perpendicular and parallel to the anisotropy axis, r is the distance between two spins, and M_z is the mean ferromagnetic moment per spin along the anisotropy axis. The Fermi wave number in this case is

affected by the magnetization, such that $k_F = \pi(1/2 - M_z)$. This means that the longitudinal spin correlation is incommensurate with the chain lattice. η is the TLL exponent that determines the dominant type of fluctuation: when $\eta > 1.0$, the longitudinal spin fluctuations always overwhelm the transverse ones, and when $\eta < 1.0$, the transverse fluctuations dominate.

The spin- $\frac{1}{2}$ XXZ Heisenberg model maps to TLL theory and can be used to explore its spin dynamics [2–4]. The relevant Hamiltonian is

$$\hat{H}_{\text{XXZ}} = J \sum_i (S_i^x S_{i+1}^x + S_i^y S_{i+1}^y + \Delta S_i^z S_{i+1}^z) - g_z \mu_0 \mu_B H \sum_i S_i^z, \quad (3)$$

where $J > 0$ is the nearest-neighbor antiferromagnetic (AFM) intrachain exchange constant, Δ is the anisotropy parameter, g_z is the component of the Landé g tensor parallel to the anisotropy axis \mathbf{z} , and H is the magnitude of the externally applied longitudinal magnetic field along \mathbf{z} . This model is exactly solvable.

In the Heisenberg-Ising regime ($\Delta > 1.0$), the solution has a gapped AFM ground state of Néel type with an easy-axis anisotropy. The characteristic excitations for this type of 1D Néel order are spinons [5,6]. A quantum phase transition

*lingjia.shen@sljus.lu.se

[†]elizabeth.blackburn@sljus.lu.se

(QPT) from the Néel state to a TLL state can be triggered by applying an external magnetic field along \mathbf{z} , at a critical field $\mu_0 H_c$. In this TLL state, η is always greater than 1 at intermediate fields, and so the primary spin fluctuations are longitudinal in nature. However, increasing the magnetic field decreases η , and when it falls below 1, transverse spin fluctuations dominate.

The TLL-type spin dynamics above $\mu_0 H_c$ have been extensively studied, both theoretically [7,8] and experimentally [9–14]. There are three types of characteristic multiparticle excitation: psinon/psinon (P/P) modes, psinon/antipsinon (P/AP) modes, and Bethe n -strings ($n = 2, 3, \dots$). While these excitations are distinct in many ways, they all form continua over well-defined regions of momentum-energy space for an ideal TLL, like the multispinon continua observed in the Néel state of isolated Heisenberg-Ising spin- $\frac{1}{2}$ chains [5]. The longitudinal dispersions of these three types of multiparticle excitation observed in experiment are in broad agreement with theoretical expectations [10,11,13]. However, certain types of TLL modes disperse in directions perpendicular to the chain [12,14]; this effect is not captured by Eq. (3).

These deviations from an ideal TLL point to the importance of interchain exchange interactions. At low fields, these interactions are responsible for the persistence of Néel ordering at finite temperatures, and the confinement of spinons; the latter transforms the spinon continua into a series of discrete Zeeman ladders [6,15]. In the field region where the TLL physics prevails, the interchain interactions give rise to two emergent magnetic orders [16–20]. Above a critical field $\mu_0 H_{c1}$, a longitudinal spin density wave (LSDW) state replaces the Néel order at sufficiently low temperatures. Whether $\mu_0 H_{c1}$ corresponds to the true quantum critical point ($\mu_0 H_c$) for the 1D Néel-TLL QPT is an open question [14]. At higher fields, when η drops below 1 [16,19], there is a second phase transition to a transverse antiferromagnetic (TAFM) state at $\mu_0 H_{c2}$. The effect of these ordering phenomena on the TLL spin dynamics is unclear and investigating this is the aim of this study.

In this paper, we report on the behavior of the TLL spin dynamics in the LSDW and TAFM phases, using $\text{SrCo}_2\text{V}_2\text{O}_8$ as our model XXZ system ($\Delta \approx 2.0$) [6,9,10]. $\text{SrCo}_2\text{V}_2\text{O}_8$ has fourfold screw chains of Co with effective spin- $\frac{1}{2}$ and Ising-like easy-axis anisotropy, which run along the crystallographic \mathbf{c} axis (Fig. 1). The LSDW develops at $\mu_0 H_{c1} = 3.9$ T and the TAFM develops at $\mu_0 H_{c2} = 7.0$ T. The incommensurability of the LSDW follows the description of the longitudinal spin correlation in Eq. (2), supporting an intimate link between this three-dimensional order and the TLL spin dynamics [16,20]. The three types of TLL multiparticle excitation discussed above have all been observed in this material above $\mu_0 H_{c1}$ [9,10,14].

In this work, the TLL spin dynamics were studied by high-resolution inelastic neutron scattering. The experimental setup used here is particularly sensitive to the longitudinal P/AP mode. We show that its line shape is *not* a continuum in the LSDW phase, especially close to the zone centers defining the static spin-spin correlations, but can instead be well defined by a damped harmonic oscillator (DHO) as though it were a single-particle excitation. It only becomes non-DHO type and continuumlike in the TAFM phase, although deviations

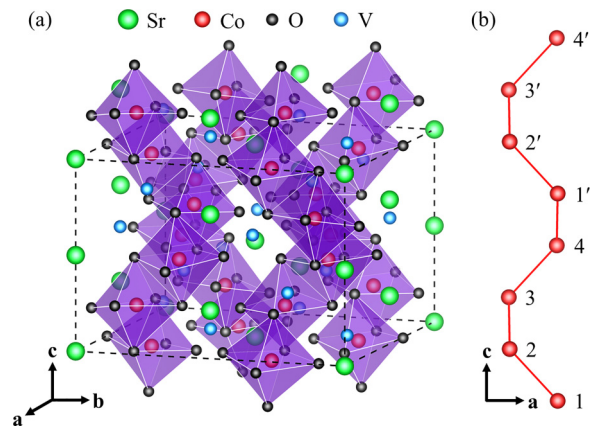


FIG. 1. Crystal structure of $\text{SrCo}_2\text{V}_2\text{O}_8$. (a) Three-dimensional atomic lattice. Unit-cell boundaries are marked by dashed lines. Shaded polygons are CoO_6 octahedra. (b) Fourfold screw chains of Co atoms in the ac plane.

from the pure 1D physics still remain. A careful study of the DHO-type longitudinal P/AP mode inside the LSDW phase also reveals a sharper but weaker response where the magnetic order parameter is strong (i.e., close to $\mu_0 H_{c1}$).

II. METHODS

Inelastic neutron scattering experiments were performed on the cold-neutron triple-axis spectrometer ThALES at the Institut Laue-Langevin (ILL) [21]. The sample, also used in Ref. [20], was a cylindrical single crystal (height 22 mm, diameter 6 mm, mass 2.7 g) grown by the floating zone method [22]. The quality of the sample was checked by neutron Laue diffraction; no impurity could be resolved.

In the experiment, the sample was mounted in a dilution refrigerator inside a 10 T vertical cryomagnet. The initial and final neutron wave vectors were selected using a PG (002) monochromator and analyzer. The final wave vector was fixed at 1.3 \AA^{-1} . The instrumental resolution in this setup is about $88 \mu\text{eV}$ in full width at half maximum (FWHM). The crystallographic \mathbf{c} axis was parallel to the vertical magnetic field to match the XXZ model [Eq. (3)]. The spin excitations were measured in the reciprocal plane $(H, K, 0)$, as used in Ref. [14]. All experimental data presented below were collected at 0.05 K.

III. EXPERIMENTAL RESULTS

In this study, we focus on the inelastic neutron scattering energy transfer spectra at $\mathbf{Q}_{\text{AFM}} = (2, 3, 0)$ and $\mathbf{Q}_{\text{FM}} = (2, 2, 0)$. \mathbf{Q}_{AFM} is a magnetic zone center for the Néel and TAFM phases, while \mathbf{Q}_{FM} is a zone center for the underlying crystal structure [14,20]. The closest magnetic zone center in the LSDW phase to \mathbf{Q}_{AFM} is $\mathbf{Q}_{\text{LSDW}} = (2, 3, \delta)$, where $\delta = 4M_z/g_z\mu_B$ [20]. This means that in a narrow field region above $\mu_0 H_{c1}$, $\mathbf{Q}_{\text{AFM}} \simeq \mathbf{Q}_{\text{LSDW}}$.

Due to the fourfold screw chain structure, the Brillouin zone in $\text{SrCo}_2\text{V}_2\text{O}_8$ is folded by a factor of four along the reciprocal \mathbf{c}^* axis, meaning that the TLL excitations at $L = 0, \frac{1}{4}, \frac{1}{2}, \text{ and } \frac{3}{4}$ can be observed simultaneously at $L = 0$

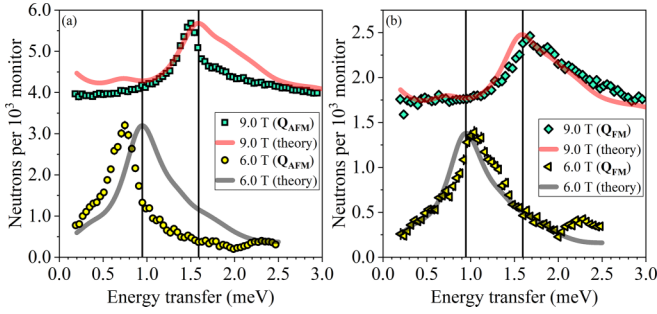


FIG. 2. Experiment vs theory comparison for the TLL spin dynamics at (a) \mathbf{Q}_{AFM} and (b) \mathbf{Q}_{FM} . The region below 0.2 meV, where the elastic peak arising from the LSDW or TAFM order prevails, has been excluded. Solid curves are theoretical line shapes for an ideal 1D TLL, which are reproduced from Ref. [10] and then scaled to match the experimental intensities. Vertical lines mark the peak positions theory curves.

[6,10,11,14]. Some additional information on the energy dispersion of the excitations between \mathbf{Q}_{AFM} and \mathbf{Q}_{FM} is reported in Ref. [14].

A peaklike feature that dominates the spectral weights above ~ 0.3 meV can be observed at all measured magnetic fields (e.g., see Fig. 2). In this energy regime (a few meV), the TLL theory predicts excitations with distinct directions, profiles, and spectral weights at $L = 0, \frac{1}{4}, \frac{1}{2},$ and $\frac{3}{4}$ [8–10]; all of them contribute to the experimental data due to the aforementioned zone folding. Assignments of the relevant modes can be helped by considering our in-plane scattering geometry, which is more sensitive to the spin fluctuations along the chain because neutrons probe the magnetic moments perpendicular to the momentum transfer. Only the longitudinal P/AP mode at $L = \frac{1}{2}$ is relatively coherent and intense. Therefore, it accounts for the dominant peaklike feature, as reported in our previous work [14]. Certain transverse modes are also expected, including Bethe 2-strings, P/AP, and P/P modes. However, their spectral weights at \mathbf{Q}_{AFM} and \mathbf{Q}_{FM} are very small due to the in-plane scattering geometry [14]. Only the relatively strong transverse modes at $L = \frac{1}{2}$ [10] will be considered in our numerical analysis (Sec. III B).

A. Deviations from an ideal 1D TLL

In Fig. 2, we show the measured spin excitations at 6.0 and 9.0 T. These data cover both LSDW and TAFM phases [20]. For comparison, we also include the theoretical predictions of Eq. (3) for an isolated spin- $\frac{1}{2}$ chain; they are reproduced from Ref. [10] and then appropriately scaled to match the experimental intensities. We find that the P/AP mode energy at \mathbf{Q}_{AFM} is softened with respect to the theoretical predictions, while that at \mathbf{Q}_{FM} is slightly hardened. This is consistent with the effect of three-dimensional magnetic ordering, which will be discussed in detail later. Moreover, the theory fails to reproduce the experimental line shape at \mathbf{Q}_{AFM} because the latter is found to be much sharper. In contrast, the experimental line shape is in better agreement with the theory at \mathbf{Q}_{FM} , except the aforementioned energy mismatch (~ 0.09 meV at both fields). At 6.0 T, a small bump can be resolved around 2.3 meV. This is the Bethe 2-string state (see below, and Refs. [10,14]).

Equation (3) predicts this mode at about 2.7 meV, which is outside our measurement window at this field.

B. Numerical model

The direct comparison with theory above showed significant deviations from an ideal TLL [8–10] in both mode line shape and energy, especially at \mathbf{Q}_{AFM} , which is very close to \mathbf{Q}_{LSDW} for the LSDW phase, and it is indeed a magnetic zone center for the TAFM phase [20]. These observations support the impact of dimensional crossover, e.g., interchain exchange interactions and three-dimensional magnetic ordering. To further describe these deviations, we have performed numerical analyses on the experimental data. We do this by fitting each mode to an analytical profile. Only those with a resolvable contribution to the inelastic neutron spectra are considered. Our numerical model is summarized below.

(i) *The elastic peak.* This was fitted using a resolution-limited Gaussian function with the area being the only adjustable parameter.

(ii) *The gapped longitudinal P/AP modes at $L = \frac{1}{2}$.* This is the strongest inelastic component in each spectrum. A DHO function with adjustable area, center, and width is used. This choice is discussed in more detail later.

(iii) *The gapped transverse Bethe 2-string modes at $L = \frac{1}{2}$.* This component is much weaker and appears in the higher end of the covered energy range, and moves out of it above 6.0 T (Fig. 3) [8,14]. A DHO function with adjustable area, center, and width is used. The center has been discussed in Ref. [14], while no magnetic field dependence can be resolved for its width and area (not shown).

(iv) *The gapless transverse continuum contributions at $L = \frac{1}{2}$.* These are approximated by a combined Lorentzian function and constant term. The Lorentzian function is centered at zero energy; its area and width are adjustable. Both terms are truncated at zero-energy transfer by a step function to reinforce the gapless nature of these excitations at $L = \frac{1}{2}$ (see the Appendix) [10]. Recently, this profile has been used to numerically reproduce the spin excitation continuum in $\text{Yb}_2\text{Pt}_2\text{Pb}$ [12].

The four components are added together and then convoluted with the experimental resolution function. The total fits are the red lines in Fig. 3, and the individual contributions are also shown. A model similar to this, but without the elastic peak term, was used by us to analyze the data above 0.3 meV and below $\mu_0 H_{c2}$ [14].

C. Line-shape changes across the LSDW-TAFM phase transition

Theoretically, the TLL modes are best described as continuum modes due to their multiparticle nature, and none of their energy line shapes can be well defined by a simple analytical form [7,8]. This means that the DHO, which can be understood as a single mode with a single decay channel [23], should not match the intrinsic line shape of the longitudinal P/AP mode (or, indeed, any other TLL modes) in an isolated XXZ chain. Nonetheless, here we use the DHO to evaluate the deviations from the theoretical expectations of 1D TLL physics revealed in Sec. III A. A similar approach has been

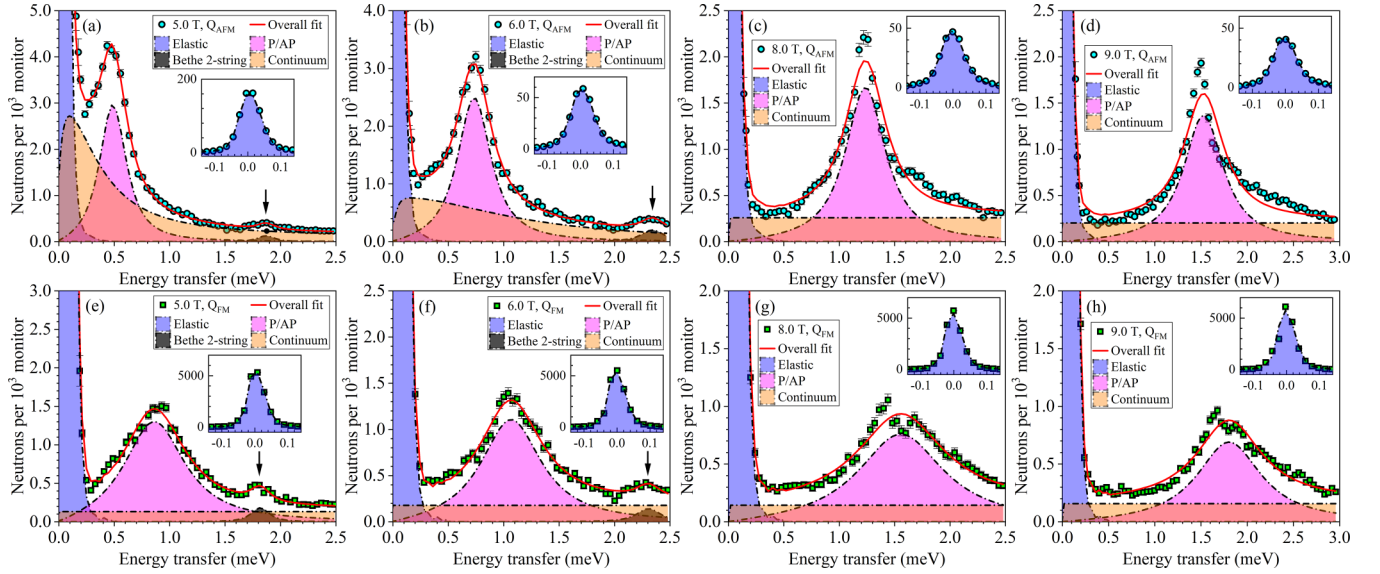


FIG. 3. The inelastic neutron scattering spectra measured at (a)–(d) the Néel/TAFM zone center $\mathbf{Q}_{\text{AFM}} = (2, 3, 0)$, and (e)–(h) the crystal zone center $\mathbf{Q}_{\text{FM}} = (2, 2, 0)$, at different magnetic fields and at a temperature of 0.05 K. The solid lines are the numerical fits described in the main text, with instrumental resolution included; the red line is the total fit and the other colors describe the four individual contributions as labeled in the legend. The black arrows mark the Bethe 2-string modes. The insets show close-up information on the elastic peaks measured at each condition, including the Gaussian fits used to characterize them.

used by Wessler *et al.* [24]. The P/AP mode dominates the measured energy spectra. If the DHO fits well, we will be able to quantitatively describe how these deviations reconstruct the mode line shape. Our numerical model also contains other terms in order to reproduce the weaker transverse modes (Sec. III B). Their spectral weights are very small (Fig. 3) and, to a good approximation, their deviations from the pure 1D TLL physics can be neglected in the current work.

A visual inspection of Fig. 3 shows that the DHO works well in the LSDW phase, but less well in the TAFM phase. In the LSDW phase, there is no additional scattering on the high-energy side of the peak, as would normally be expected for the excitations at the start of a continuum [24]. The other modes included in our fit have much smaller spectral weights, and so even if they are picking up some additional scattering from a long tail on the longitudinal P/AP signal, this is still too small to affect the overall P/AP line shape.

Above $\mu_0 H_{c2}$, however, the DHO function fails to fit the P/AP mode. To assess the discrepancy, we calculate the adjusted R -squared value,

$$R_{\text{adj}}^2 = 1 - (1 - R^2) \frac{n_d - 1}{n_d - n_p - 1}, \quad (4)$$

where R^2 is the coefficient of determination, n_d is the number of individual data points, and n_p is the number of fitting parameters. In this calculation, we have excluded the data below 0.3 meV to minimize the effect of the elastic peak contributions. For this reason, we have also excluded the spectrum at \mathbf{Q}_{AFM} and 4.0 T, where this mode is located below 0.3 meV [Fig. 5(b)]. As shown in Fig. 4, the R_{adj}^2 values at both \mathbf{Q}_{AFM} and \mathbf{Q}_{FM} undergo a sharp, sizable reduction on entering the TAFM phase. Below $\mu_0 H_{c2}$, the R_{adj}^2 values at \mathbf{Q}_{AFM} are always closer to 1.0 (a perfect fit) than those at \mathbf{Q}_{FM} . Since \mathbf{Q}_{AFM} is in close vicinity of \mathbf{Q}_{LSDW} [20], these observations

suggest that the static spin-spin correlations in the LSDW state, which are strong close to \mathbf{Q}_{LSDW} , stabilizes the DHO-type longitudinal P/AP mode. Again, we emphasize that the purpose of this analysis is *not* to reproduce the line shape of the longitudinal P/AP mode at all fields, but to highlight how the mode behavior deviates from the theoretical descriptions for an ideal TLL. A complete description of the line shape in the TAFM phase is outside the scope of this paper.

D. Longitudinal P/AP mode in magnetic field

Although the DHO function only describes the longitudinal P/AP mode well in the LSDW phase, it still provides an

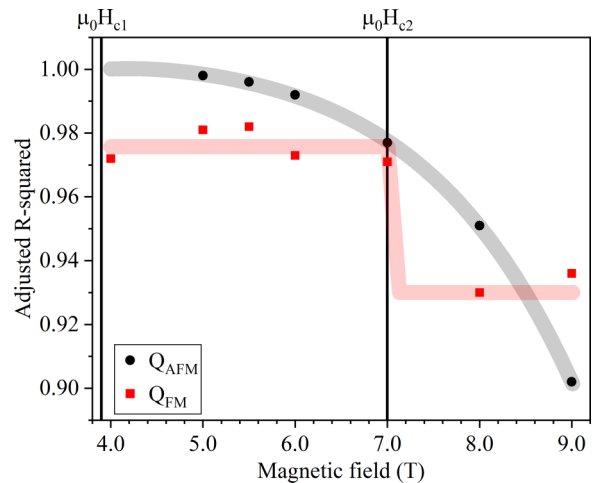


FIG. 4. The adjusted R -squared value [Eq. (4)] for the fits illustrated in Fig. 3 as a function of magnetic field. $\mu_0 H_{c1}$ and $\mu_0 H_{c2}$ (main text) are indicated by vertical lines. The thick shaded lines are guides for the eye.

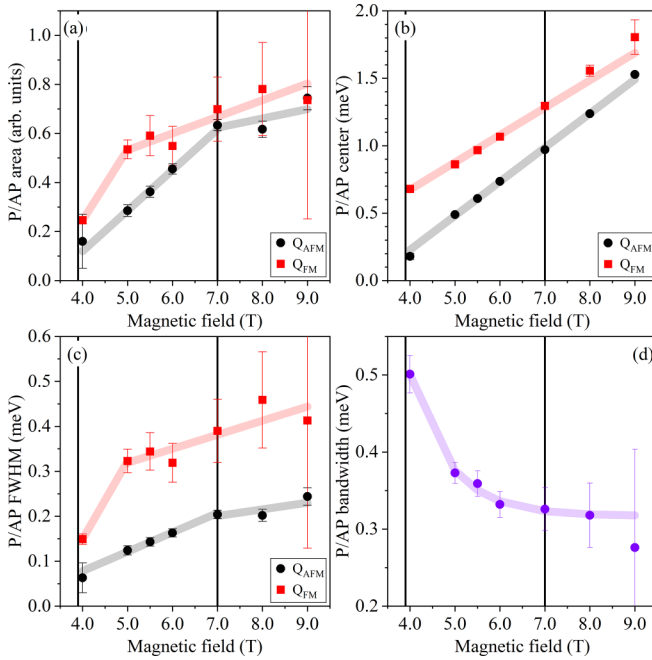


FIG. 5. The fitted parameters of the DHO used to describe the longitudinal psinon/antipsinon (P/AP) mode, as a function of magnetic field. The parameters shown are (a) the area, (b) the center, (c) the full width at half maximum (FWHM), and (d) the effective bandwidth, defined as the energy difference between the mode energies at the two zone centers. The vertical lines mark $\mu_0 H_{c1}$ and $\mu_0 H_{c2}$ (main text). The thick shaded curves are guides for the eye.

informative parametrization of the behavior of the excitations in the TAFM phase, and so now we consider how these parameters vary across the field range that is examined here (Fig. 5).

1. Spectral weight

At 4.0 T, which is 0.1 T above $\mu_0 H_{c1}$, the DHO areas, or spectral weights, at \mathbf{Q}_{AFM} and \mathbf{Q}_{FM} are small [Fig. 5(a)]. At \mathbf{Q}_{AFM} and intermediate magnetic fields, the area increases approximately linearly. A kink develops at $\mu_0 H_{c2}$, beyond which the field-induced variation is greatly suppressed. At \mathbf{Q}_{FM} , the area appears to increase approximately linearly over the whole field range, although data points above 9.0 T in the TAFM phase are lacking. The exception to this is the measurement at 4.0 T, and this will be revisited later. There is no resolvable kink at $\mu_0 H_{c2}$.

We can also see that the uncertainties of the P/AP area in the TAFM phase are larger than those in the LSDW phase, especially for the data at \mathbf{Q}_{FM} . An examination of the covariance-variance matrices in the numerical analysis reveals strong correlations between the P/AP area and width parameters (not shown). The latter also has larger uncertainties in the TAFM phase [Fig. 5(c)]. In our model, the P/AP excitations are represented by a DHO (Sec. III B). The DHO captures the P/AP profile less well in the TAFM phase (Fig. 4, Sec. III C), explaining the larger uncertainties that are observed.

We attempt to interpret these observations based on the scenario where the LSDW mainly results from the partial condensation of the longitudinal P/AP mode at \mathbf{Q}_{LSDW} . Such a condensation is favored because this mode is intrinsically

gapless at \mathbf{Q}_{LSDW} [8,10,11]. Two effects are expected when increasing the magnetic field in the LSDW state.

First, the LSDW order parameter gets weakened [17,20]. This enhances the fluctuating moment. Second, \mathbf{Q}_{AFM} gradually becomes experimentally distinct from \mathbf{Q}_{LSDW} . Consequently, the amount of condensed longitudinal P/APs at \mathbf{Q}_{AFM} decreases. Both effects can “free” the condensed longitudinal P/APs at \mathbf{Q}_{AFM} . Accordingly, the DHO area is increased. The LSDW state is fully suppressed at $\mu_0 H_{c2}$. The TAFM state at higher fields comes from the condensed transverse spin fluctuations. This means that the longitudinal P/AP mode is less sensitive to the order in this phase, so that the effect of increased field is weakened, giving rise to a kink at $\mu_0 H_{c2}$.

\mathbf{Q}_{FM} is a crystal zone center, making the longitudinal P/APs there less sensitive to the interaction with the ordered magnetic moment at \mathbf{Q}_{LSDW} . We suggest that this explains the weaker field dependence of the spectral weight from 5.0 T upwards, which is similar to that seen in the TAFM state for \mathbf{Q}_{AFM} . However, this cannot explain the suppressed DHO area at 4.0 T. Since this field is only 0.1 T above $\mu_0 H_{c1}$, we suggest that the criticality underlying the Néel-LSDW phase transition plays a role here. In other words, we speculate that the longitudinal P/AP mode is suppressed everywhere in the momentum space in the close vicinity of $\mu_0 H_{c1}$.

2. Dispersion

The centers of the longitudinal P/AP mode obtained from the DHO fitting are plotted in Fig. 5(b). Previously, similar data have been reported for the longitudinal P/AP mode at (2.3, 2.3, 0) [10], where the mode center lies between those at \mathbf{Q}_{AFM} and \mathbf{Q}_{FM} [14]. This mode is always softer at \mathbf{Q}_{AFM} . At both zone centers, the variation as a function of field is approximately linear, albeit with slightly different slopes.

Next, we consider the effective bandwidth. This parameter is equal to the difference between the DHO center positions at \mathbf{Q}_{AFM} and \mathbf{Q}_{FM} [Fig. 5(d)] [14]. The longitudinal P/AP band is broadest close to $\mu_0 H_{c1}$ (~ 0.50 meV), and gradually decreases to about 0.32 meV at $\mu_0 H_{c2}$, staying approximately constant up to the highest field that is probed (9.0 T). The finite bandwidth reveals that the longitudinal P/APs are not solitonic perpendicular to the chains. In other words, the inter-chain P/AP-P/AP correlations are significant in $\text{SrCo}_2\text{V}_2\text{O}_8$. The underlying interactions are responsible for the deviations from the pure 1D TLL physics. Since the bandwidth varies strongly with magnetic field, these interactions are less likely to come solely from the conventional direct or indirect exchange integrals, which are determined by the crystal structure. We propose that they scale with the molecular field generated by the bulk magnetic order parameter. As reported in Ref. [20], the LSDW order weakens on approaching $\mu_0 H_{c2}$. Between $\mu_0 H_{c2}$ and 9.0 T, the change in the TAFM order parameter is small.

3. Linewidth

For an ideal DHO, the FWHM is inversely proportional to the lifetime of the mode. As shown in Fig. 5(c), the longitudinal P/AP mode at \mathbf{Q}_{AFM} is sharper than that at \mathbf{Q}_{FM} over the entire magnetic field window that is probed. This is clearly illustrated in Fig. 6, where the FWHM is plotted for

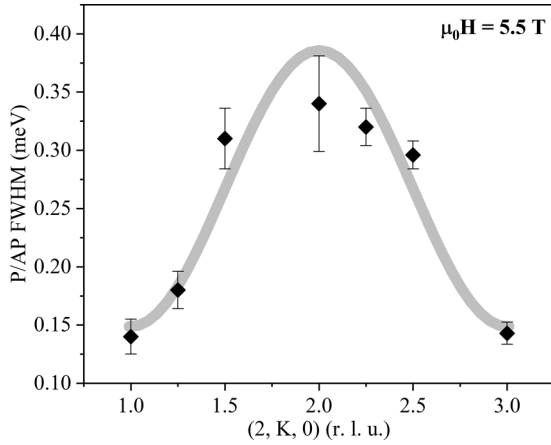


FIG. 6. The FWHM of the DHO profile describing the longitudinal P/AP mode as a function of momentum transfer at 5.5 T. $K = 1.0$ and 3.0 are Néel/TAFM zone centers. The thick shaded line is a guide for the eye.

a range of momentum transfer values measured at 5.5 T (in the LSDW phase). The mode sharpens close to momentum transfers where $H + K + L = \text{odd integer}$; these positions are closer to the corresponding magnetic zone centers of the LSDW phase [20]. These results strongly suggest that at least in the LSDW phase where the longitudinal P/AP mode well resembles a DHO, its lifetime at a given magnetic field is prolonged by the static magnetic correlations.

We now discuss the magnetic field effect on the linewidth. For both \mathbf{Q}_{AFM} and \mathbf{Q}_{FM} , the P/AP mode is sharpest at 4.0 T. As the magnetic field increases, the mode FWHM gets broadened [Fig. 5(c)]. This supports field-enhanced damping. In the TAFM phase, the mode becomes too damped, or additional damping channels emerge, so that it is no longer a DHO. This partially recovers the continuumlike line shape.

One important factor in the quasi-1D systems of this class, which is not captured by the XXZ model [Eq. (3)], is the molecular field generated by neighboring chains due to three-dimensional magnetic ordering. This effect has been studied for the spinon line-shape reconstruction in the Néel state [6,14,15,25]. We are not aware of any theoretical framework addressing the impact of such effect on the TLL spin dynamics. We suggest one possible scenario for understanding the behavior of the longitudinal P/AP linewidth. Its magnetic field dependence is reminiscent of that of the spinon mode in the bulk Néel state [14]. In the latter case, below $\mu_0 H_{c1}$, the spinon continuum expected for an isolated spin chain is sharpened by the interchain molecular field [6,14,15,25]; the field-enhanced damping is related to the weakening of the magnetic order parameter or the generation of magnetic inhomogeneities (spin flips). Similarly, the linewidth of the longitudinal P/AP mode above $\mu_0 H_{c1}$ could also be controlled by the LSDW or TAFM order parameter. However, additional complications arise due to the complex magnetic structures of the LSDW and TAFM phases [17,18]. In particular, the LSDW has an incommensurate structure with easy-axis anisotropy, while TAFM is commensurate with predominantly easy-plane anisotropy. In order to thoroughly understand the longitudinal P/AP linewidth, the molecular fields in the corresponding regions need to be studied.

IV. CONCLUSION

In summary, we have used inelastic neutron scattering to study the TLL-type spin dynamics in the quasi-1D quantum magnet $\text{SrCo}_2\text{V}_2\text{O}_8$. We identify a strong response of the longitudinal P/AP mode to the LSDW and TAFM phases, as well as their underlying interchain magnetic correlations. In particular, this mode resembles a damped harmonic oscillator in the LSDW phase and close to its magnetic zone center, which is in stark contrast to the continuous line-shape prediction for isolated spin chains [8,10]. Furthermore, we show that the three-dimensional magnetic ordering weakens the spectral weight, promotes the in-plane dispersion, and sharpens the spectral linewidth of the longitudinal P/AP mode, especially in the LSDW phase. All these observations stress the importance of dimensional crossover, which has only been treated on the mean-field level in the literature [6,14,25]. We also observe some evidence suggesting a response in some transverse TLL modes (see the Appendix). Further studies are demanded for clarifying the relevant questions.

The data collected at the ILL are available [21].

ACKNOWLEDGMENTS

L.S., E.C., and E.B. acknowledge financial support from the Swedish Research Council under Contract No. 2018-04704. A.A. acknowledges support from the Crafoord Foundation, Dnr. 20190930. D.P. and A.T.B. acknowledge the U.K. Engineering and Physical Sciences Research Council for funding under Grant No. EP/N034872/1. The authors gratefully acknowledge the ILL for the allocated beam time.

APPENDIX: TRANSVERSE CONTINUUM IN MAGNETIC FIELD

In addition to the strong and relatively sharp longitudinal P/AP feature studied in the main text, there is also a much weaker and broader feature that can be assigned as a continuum. We argue that it is transverse in nature on the basis of

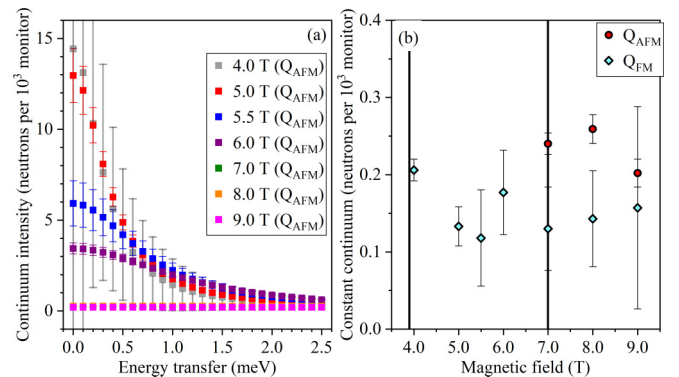


FIG. 7. The magnetic field dependence of the transverse continuum contributions. (a) Combined Lorentzian+constant term at \mathbf{Q}_{AFM} . (b) Constant at \mathbf{Q}_{FM} . Those at \mathbf{Q}_{AFM} inside the TAFM phase are also included for comparison. The vertical solid lines mark $\mu_0 H_{c1}$ and $\mu_0 H_{c2}$.

numerical calculations [8,10]. In $\text{SrCo}_2\text{V}_2\text{O}_8$, the transverse modes at $L = 0, \frac{1}{4}, \frac{1}{2}$, and $\frac{3}{4}$ can be simultaneously probed at $(H, K, 0)$ due to the Brillouin zone folding [10]. In our horizontal scattering geometry, which is most sensitive to the longitudinal TLL spin dynamics because neutrons probe the magnetic fluctuations perpendicular to the momentum transfer, there are two candidates for generating a resolvable transverse response: the gapless P/AP at $L = \frac{1}{2}$ and the gapless P/P at $L = \frac{1}{2}$. It is impossible to separate these two continua in our data.

For the purposes of our fit, we include two terms, a Lorentzian function centered at zero energy and a constant; both are truncated at zero energy to reinforce the gapless nature [8,10]. Mathematically, this combined term is necessary because, in the case of a very broad continuum, the profile will appear as a constant in the probed energy window, and so the Lorentzian is no longer able to describe it adequately.

The transverse continuum contribution is illustrated in Fig. 7. At \mathbf{Q}_{FM} , only an almost field-independent constant profile is present [Figs. 3(e)–3(h), Fig. 7(b)]; no Lorentzian profile can be resolved. At \mathbf{Q}_{AFM} , the continuum is dominated by the Lorentzian profile inside the LSDW state [Fig. 7(a)]. The enormously large uncertainties for the data at 4.0 T are caused by the strong correlations between the Lorentzian and Gaussian profiles. The latter describes the elastic line (Sec. III B) and overwhelms the spectral weights below 0.3 meV, where most spectral weights of the Lorentzian-type continuum at 4.0 T are located [Fig. 3(a)]. Phenomenologically, it is clear that the Lorentzian contribution gets gradually suppressed while approaching $\mu_0 H_{c2}$. Only the constant profile persists into the TAFM phase, the amplitude of which is similar to those at \mathbf{Q}_{FM} [Fig. 7(b)]. From this, we conclude that the LSDW-TAFM transition only affects the transverse continua at \mathbf{Q}_{AFM} .

-
- [1] T. Giamarchi, *Quantum Physics in One Dimension*, International Series of Monographs on Physics (Clarendon Press, Oxford, 2004).
- [2] F. D. M. Haldane, General Relation of Correlation Exponents and Spectral Properties of One-Dimensional Fermi Systems: Application to the Anisotropic $S = \frac{1}{2}$ Heisenberg Chain, *Phys. Rev. Lett.* **45**, 1358 (1980).
- [3] C. N. Yang and C. P. Yang, One-dimensional chain of anisotropic spin-spin interactions. I. Proof of Bethe's hypothesis for ground state in a finite system, *Phys. Rev.* **150**, 321 (1966).
- [4] N. Bogoliubov, A. Izergin, and V. Korepin, Critical exponents for integrable models, *Nucl. Phys. B* **275**, 687 (1986).
- [5] J.-S. Caux, J. Mossel, and I. P. Castillo, The two-spinon transverse structure factor of the gapped Heisenberg antiferromagnetic chain, *J. Stat. Mech.* (2008) P08006.
- [6] A. K. Bera, B. Lake, F. H. L. Essler, L. Vanderstraeten, C. Hubig, U. Schollwöck, A. T. M. N. Islam, A. Schneidewind, and D. L. Quintero-Castro, Spinon confinement in a quasi-one-dimensional anisotropic Heisenberg magnet, *Phys. Rev. B* **96**, 054423 (2017).
- [7] M. Karbach and G. Müller, Line-shape predictions via Bethe ansatz for the one-dimensional spin- $\frac{1}{2}$ Heisenberg antiferromagnet in a magnetic field, *Phys. Rev. B* **62**, 14871 (2000).
- [8] W. Yang, J. Wu, S. Xu, Z. Wang, and C. Wu, One-dimensional quantum spin dynamics of Bethe string states, *Phys. Rev. B* **100**, 184406 (2019).
- [9] Z. Wang, J. Wu, W. Yang, A. K. Bera, D. Kamenskyi, A. T. M. N. Islam, S. Xu, J. M. Law, B. Lake, C. Wu, and A. Loidl, Experimental observation of Bethe strings, *Nature (London)* **554**, 219 (2018).
- [10] A. K. Bera, J. Wu, W. Yang, R. Bewley, M. Boehm, J. Xu, M. Bartkowiak, O. Prokhnenko, B. Klemke, A. T. M. N. Islam, J. M. Law, Z. Wang, and B. Lake, Dispersions of many-body Bethe strings, *Nat. Phys.* **16**, 625 (2020).
- [11] Q. Faure, S. Takayoshi, V. Simonet, B. Grenier, M. Månsson, J. S. White, G. S. Tucker, C. Rüegg, P. Lejay, T. Giamarchi, and S. Petit, Tomonaga-Luttinger Liquid Spin Dynamics in the Quasi-One-Dimensional Ising-Like Antiferromagnet $\text{BaCo}_2\text{V}_2\text{O}_8$, *Phys. Rev. Lett.* **123**, 027204 (2019).
- [12] W. J. Gannon, I. A. Zaliznyak, L. S. Wu, A. E. Feiguin, A. M. Tsvelik, F. Demmel, Y. Qiu, J. R. D. Copley, M. S. Kim, and M. C. Aronson, Spinon confinement and a sharp longitudinal mode in $\text{Yb}_2\text{Pt}_2\text{Pb}$ in magnetic fields, *Nat. Commun.* **10**, 1123 (2019).
- [13] L. S. Wu, S. E. Nikitin, Z. Wang, W. Zhu, C. D. Batista, A. M. Tsvelik, A. M. Samarakoon, D. A. Tennant, M. Brando, L. Vasylechko, M. Frontzek, A. T. Savici, G. Sala, G. Ehlers, A. D. Christianson, M. D. Lumsden, and A. Podlesnyak, Tomonaga-Luttinger liquid behavior and spinon confinement in YbAlO_3 , *Nat. Commun.* **10**, 698 (2019).
- [14] L. Shen, E. Campillo, O. Zaharko, P. Steffens, M. Boehm, K. Beauvois, B. Ouladdiaf, Z. He, D. Prabhakaran, A. T. Boothroyd, and E. Blackburn, Inhomogeneous spin excitations in weakly coupled spin- $\frac{1}{2}$ chains, *Phys. Rev. Res.* **4**, 013111 (2022).
- [15] H. Shiba, Quantization of magnetic excitation continuum due to interchain coupling in nearly one-dimensional ising-like antiferromagnets, *Prog. Theor. Phys.* **64**, 466 (1980).
- [16] K. Okunishi and T. Suzuki, Field-induced incommensurate order for the quasi-one-dimensional XXZ model in a magnetic field, *Phys. Rev. B* **76**, 224411 (2007).
- [17] E. Canévet, B. Grenier, M. Klanjšek, C. Berthier, M. Horvatić, V. Simonet, and P. Lejay, Field-induced magnetic behavior in quasi-one-dimensional Ising-like antiferromagnet $\text{BaCo}_2\text{V}_2\text{O}_8$: A single-crystal neutron diffraction study, *Phys. Rev. B* **87**, 054408 (2013).
- [18] B. Grenier, S. Petit, V. Simonet, E. Canévet, L.-P. Regnault, S. Raymond, B. Canals, C. Berthier, and P. Lejay, Longitudinal and transverse Zeeman ladders in the Ising-like chain antiferromagnet $\text{BaCo}_2\text{V}_2\text{O}_8$, *Phys. Rev. Lett.* **114**, 017201 (2015).
- [19] M. Klanjšek, M. Horvatić, S. Krämer, S. Mukhopadhyay, H. Mayaffre, C. Berthier, E. Canévet, B. Grenier, P. Lejay, and E. Orignac, Giant magnetic field dependence of the coupling between spin chains in $\text{BaCo}_2\text{V}_2\text{O}_8$, *Phys. Rev. B* **92**, 060408(R) (2015).
- [20] L. Shen, O. Zaharko, J. O. Birk, E. Jellyman, Z. He, and E. Blackburn, Magnetic phase diagram of the quantum spin

- chain compound $\text{SrCo}_2\text{V}_2\text{O}_8$: A single-crystal neutron diffraction study, *New J. Phys.* **21**, 073014 (2019).
- [21] L. Shen, E. Blackburn, M. Boehm, A. Boothroyd, E. Campillo, D. Prabhakaran, P. Steffens, and D. M. Vasiukov, *Critical Magnetic Excitations Beyond the Tomonaga-Luttinger Liquid Description in a Heisenberg-Ising Quantum Spin Chain Antiferromagnet* (Institut Laue-Langevin, 2019).
- [22] P. Lejay, E. Canevet, S. Srivastava, B. Grenier, M. Klanjsek, and C. Berthier, Crystal growth and magnetic property of $M\text{Co}_2\text{V}_2\text{O}_8$ ($M = \text{Sr}$ and Ba), *J. Cryst. Growth* **317**, 128 (2011).
- [23] B. Fåk and B. Dorner, Phonon line shapes and excitation energies, *Phys. B: Condens. Matter* **234-236**, 1107 (1997).
- [24] C. Wessler, B. Roessli, K. W. Krämer, B. Delley, O. Waldmann, L. Keller, D. Cheptiakov, H. B. Braun, and M. Kenzelmann, Observation of plaquette fluctuations in the spin-1/2 honeycomb lattice, *npj Quantum Mater.* **5**, 85 (2020).
- [25] S. E. Nagler, W. J. L. Buyers, R. L. Armstrong, and B. Briat, Ising-like spin-1/2 quasi-one-dimensional antiferromagnets: Spin-wave response in CsCoX_3 salts, *Phys. Rev. B* **27**, 1784 (1983).